Effect of Blade Pitch Angle on a 2-Bladed Horizontal Axis Tidal Current Turbine Performance

Ramin Alipour[1], Roozbeh Alipour[1], Farhad Fardian[1], Seyed Saeid Rahimian Koloor[2], Reza Moezzi[2*]

[1] Department of Mechanical Engineering, Mahshahr Branch, Islamic Azad University, Mahshahr, Iran

[2] Institute for Nanomaterials, Advanced Technologies and Innovation, Technical University of Liberec, Studentska 2, Liberec, 461 17, Czech Republic

Reza.Moezzi@tul.cz

Abstract. Horizontal axis tidal current turbine (HATCT) is one of the strongest devices to generate electricity using the hydraulic flow. These devices need to act under an optimum blade pitch angle to prevent power losses. In the present work, the blade element momentum theory (BEM) was used to initial design of a 2-Bladed HATCT. The turbine was modeled in -60 till +60 blade pitch angle and the performance of the turbine at the tip speed ratios (TSRs) between 4 to 6 was assessed through a computational fluid dynamic (CFD) analysis. The outputs were pressure contours, turbulence kinetic energy (TKE) contours, streamlines, torque, and power coefficient curves (Cp). Our novel and considerable results showed the maximum amount of Cp is 0.29 in 00 blade pitch angle at TSR 5 which prevents power losses significantly. Also, it is possible to improve performance by setting blades pitch angles in different TSRs.

Keywords: Horizontal axis tidal current turbine, Power coefficient, Tip Speed Ratio (TSR), Blade pitch angle, CFD.

1 Introduction

Tidal current technology is one of the most adequate ways to use renewable energy for reducing environmental pollution [1]. It is more predictable and controllable in compression with solar cells, tidal waves, wind, etc. [2, 3]. HATCTs are able to generate more power with respect to the vertical axis turbines in hydrokinetics turbine types [4, 5]. There have been several projects available to develop HATCTs for commercial applications e.g. MeyGen, West Islay, and SR2000 [6-8]. Many researchers have studied different aspects of HATCTs design such as wake [9] and farm [10, 11]. Hee Jo et al. [12], designed a 2-Bladed HATCT based on the BEM-CFD method with a 10 m diameter (D) and showed 86% of velocity design improvement at 18D downstream. A new insight into tidal turbines was introduced by Tarver et al. [13] who determined that by reducing the turbine diameter and arranging them into a vertical array, the value of C_p increases. It is of particular importance to set an optimum condition for a turbine when it is located against the flow, so researchers have tried to recognize the maximum amount of C_p for a single turbine. Hee Jo et al. [14], studied the performance of 3-Bladed HATCTs to investigate the efficiency of the turbine under different TSRs. In

M. Petr et al. (eds.), *62nd International Conference of Machine Design Departments (ICMD 2022)*, Atlantis Highlights in Engineering 28,
https://doi.org/10.2991/978-94-6463-423-5_22

contrast with wind flow which raises from the pressure difference, water flow is created due to the gravity and gush from higher to lower energy levels. So, it is important to assess the performance of these turbines under different depths and bed slop. Münch-Alligné et al. [15], designed a new hydrokinetic turbine for the river usage and showed the performance of the turbine increases with the depth and the tilt. On the other hand, Yan et al. [16] showed there is no significant changes for C_p after shallow-tip immersion under free surface wave condition. The number of blades is the other important parameter to design HATCTs since the turbines with different blade number have distinct performance. Also, it is essential to know why and when engineers need to install a turbine with a specific number of the blades. Therefore, in a comprehensive numerical study, Alipour et al. [17] illustrated that with increase the number of blades, the value of C_p improves at the lower TSR .

In recent years, studies have focused on improving the performance of HATCTs by designing the optimum blades. Goundar and Ahmed [18] designed a HATCT using different hydrofoils along with the blade. Bi-directional counter-rotating type of HATCT was purposed by Huang et al. [19] in the way of symmetrical hydrofoils. The neural network model was used to design a blade by Zhu et al. [20] for enhancing the performance of HATCTs.

It has been reported that pitch-able HATCTs are useful for the stability of the C_p due to the fluctuation of current velocity for avoiding energy losses resulted from attack angle control [21]. In this case, the present authors only could find single research that has specifically addressed the effect of blade pitch angle on the performance of HATCTs through an experimental investigation [22]. This recent report indicated that with increasing the blade pitch angle from the optimum value, power and thrust decrease so that reducing the thrust is more obvious than the power.

In this paper, the effect of blade pitch angle from -6^0 till $+6^0$ for TSR $4 \leq TSR \leq 6$, is assessed computationally. A numerical simulation using the CFD approach through ANSYS-FLUENT software is conducted as a computer assisted method. The results included pressure contours, TKE contours, streamlines, torque, and C_p for different blade pitch angles and TSRs. The results and conclusions are helpful for developers who intend to fabricate pitch able HATCTs.

2 Physical model

Design data was extracted using the BEM method [12, 14] and turbine geometrical modeling was implemented assisting Solidworks software. Fig 1. shows the components of the turbine against the flow. To survey optimum performance, the turbine was designed in different blade pitch angles from -6^0 to 6^0. Fig 2. depicts the clockwise direction gives a positive blade pitch angle and contour-clockwise provides a negative blade pitch angle. Fig 3. presents the distribution of attack angle caused by blade pitch angle changes. As it is obvious, the attack angle decreases by increasing the blade pitch angle and vice versa.

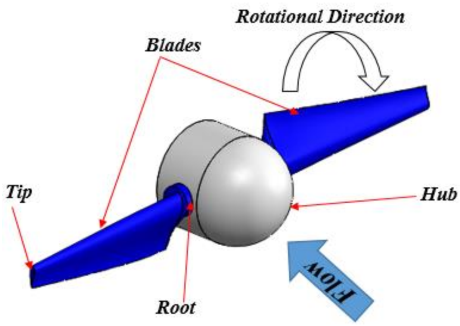

Fig 1: Components of HATCTs against the flow

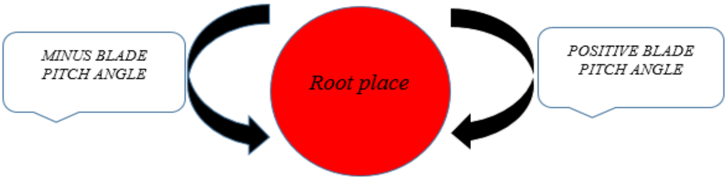

Fig 2: Rotational direction for blade pitch angle

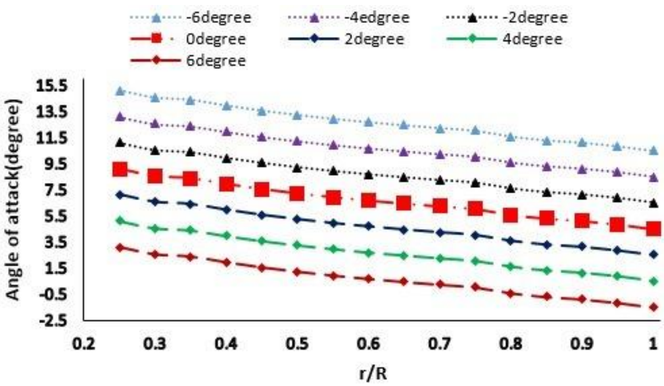

Fig 3: Distribution angle of attack due to blade pitch angle variation

3 Numerical Simulation

In this study, the computational domain was performed using Solidworks as shown in Fig 4. For numerical simulation, the CFD approach was used through ANSYS-FLUENT software. The turbulence model was applied based on the SST-k-ω model [23]. This model has been widely employed in the simulation of turbomachines and tidal current turbines [12, 14, 24]. Also, it consists of k-ω and k-ε models for close to the wall and beyond the wall and respectively. The simulations were validated against the experimental [14] and computational [17] studies reported in the literature. A moving reference frame was applied to the interface condition between the rotating area and the fluid domain. Velocity inlet (initially 1 m/s) and gauge pressure (initially zero pascal) were considered as the inlet and outlet boundary conditions of the fluid domain, respectively. The symmetry condition was applied for the free surface, and the wall condition was dedicated to the walls. These boundary conditions are presented in Fig 5. To have a precise estimation of the torque, a dense layer of unstructured mesh was used, and 10 layers of inflation were performed on the boundary layer areas. Fig 6. shows the vertical section for the computational fluid domain and boundary layer around the turbine.

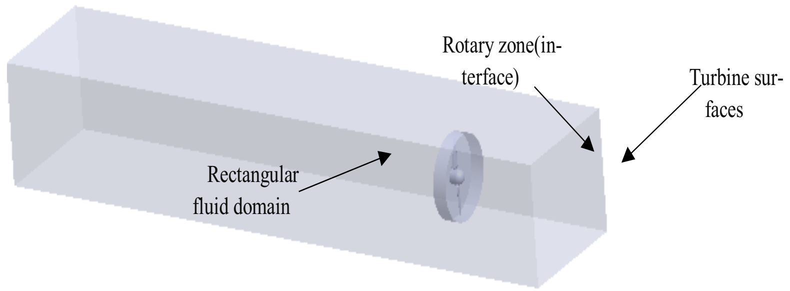

Fig 4: Turbine computational domain

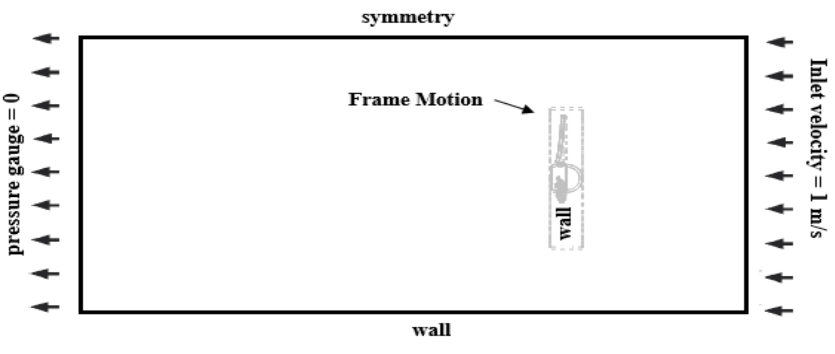

Fig 5: Boundary conditions

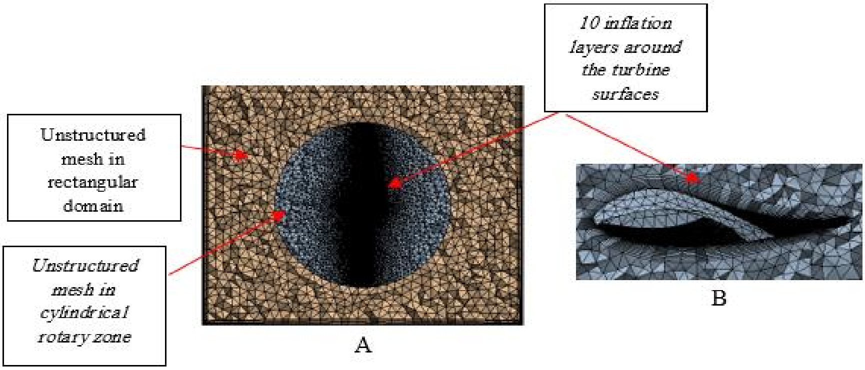

Fig 6: Mesh A) Vertical section, B) Inflation around the blade

4 Performance of the turbine

Turbines convert energy from a fluid into electricity and their performance evaluation is assessed with the value of energy generation. Geometry features, free stream velocity, and angular velocity are the main characteristics of the assessment of turbine efficiency [12]. So, the TSR parameter is available to define the operational condition of the turbine as follows

$$TSR = \frac{\omega . R}{V} \tag{1}$$

where ω, R, and V are angular velocity, the total radius of the blade from tip to root, and the free stream velocity, respectively. C_P is obtained as Eq (2)

$$C_P = \frac{P}{0.5 \rho A V^3} \tag{2}$$

where ρ is the fluid density, A is the rotor area, and P is the power generation by the turbine that calculates through Eq (3):

$$P = T . \omega \tag{3}$$

In Eq (3), T is the torque. Substituting Eq. (3) in Eq (2), C_P can be calculated as follows

$$C_P = \frac{T . \omega}{.5 \rho A V^3} \tag{4}$$

5 Results and discussion

5.1 Validation of CFD work

In the previous work [17], to assure the simulation is accurate, after mesh convergence study, the amount of torque extracted from CFD analysis and consequently C_p were compared by experimental results [14, 25, 26]. The number of errors approximately was about 10% which is in good agreement with experiments. The main reason for this difference was the energy losses in the experimental model due to gears and bearings that were not considered in the CFD simulation [4].

5.2 Pressure contours

Fig 7. shows the pressure contours around the airfoils. For all models, the maximum amount of pressure is occurred in the leading-edge area due to the minimum velocity caused by the fluid-blade incident. After passing the flow from the leading-edge, the pressure decreases due to an increase in velocity. As Fig. 7 shown, by increasing the bladed pitch angle from -6^0 to +6^0 the attack angle reduces, so the point of separation gradually distances from the leading edge and it moved toward the trailing edge in the suction pressure area. Passing through 0^0 blade pitch angle the amount of pressure increases in the maximum thickness of the pressure side area and decreasing pressure differences between both sides lead to a decrease in the amount of lift and torque is reduced.

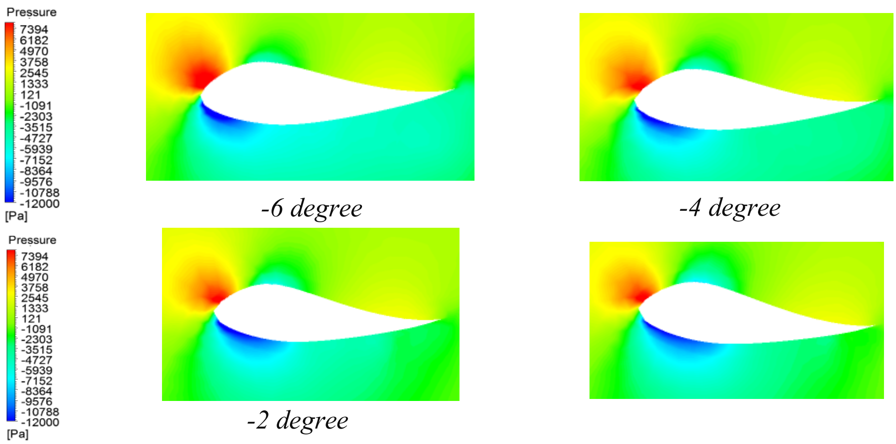

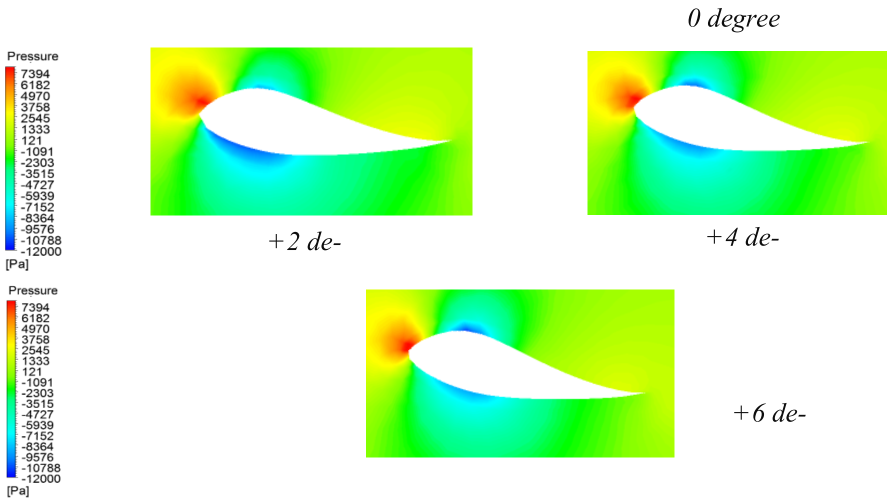

Fig 7: Contours of pressure around the airfoils at TSR = 5

5.3 Turbulence kinetic energy (TKE)

Fig 8. shows the TKE contours at TSR = 6, for different blade pitch angles. In -6^0 blade pitch angles, the value of attack angle is high, and the lift decreases that causes a reduction in the torque. By increasing the blade pitch angle towards the range 0^0 to $+2^0$, the airfoil acts in the range of maximum lift to drag ratio and the torque enhances. After $+2^0$, the blade pitch angle decreases which leads to a decrease in the attack angle, hence the flow starts to fall off from the leading edge, and the separation area for the pressure side gradually increases. As the result, the drag generated due to the TKE increases, leads to detract the amount of lift to drag ratio and consequently the torque decreases.

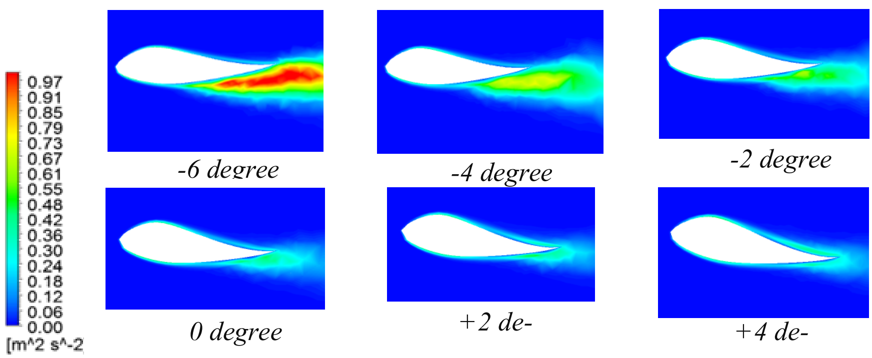

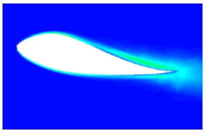

+6 de-

Fig 8: TKE contours in various blade pitch angle at TSR = 6

5.4 Streamlines

Fig 9. depicts the streamlines around the blade for $4 \leq TSR \leq 6$ in 0^0 blade pitch angle. For TSR 4, flow separation can be observed. By increasing the TSR, the attack angle reduces, so it causes to decrease in separation around the blade. If the tip speed ratio goes less than 5, the blade is situated with a larger attack angle than that of the maximum lift to drag ratio, the blade is closed to stall condition and torque is reduced. If the tip speed ratio goes up more than 5, lift decreases, and the lift to drag ratio is distanced from the maximum lift to drag ratio and torque reduces. So the maximum amount of torque can be observed in TSR 5 when the maximum lift to drag ratio occurs.

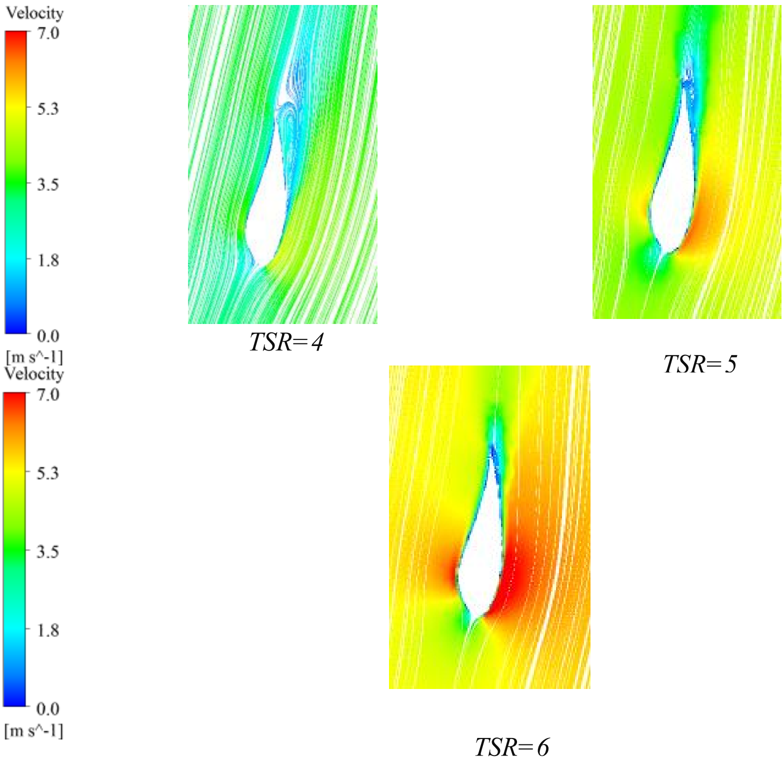

Fig 9: Streamlines at different TSRs for 0^0 blade pitch angle

5.5 Torque and power coefficient

Fig 10. shows the torque versus to blade pitch angle for 4≤TSR≤6. The amount of torque has more stable in TSR 5. By increasing angular velocity till TSR 6, the amount of attack angle is reduced, besides increasing the blade pitch angle the attack angle goes down, so the combination of increasing in TSR and blade pitch angle after -2^0 lead to extremely decreases attack angle. In this situation drag caused by turbulence increases, therefore the amount of torque reduces and the minimum amount of torque occurred in TSR 6 and 6^0 blade pitch angle.

By decreasing in TSR till 4, the amount of attack angle is increased, also by decreasing the blade pitch angle the attack angle goes up, so the combination of decreasing in TSR and blade pitch angle lower than +2^0, the attack angle extremely increases. In this situation, the turbine acts near the stall condition, so the value of torque is dramatically dropping in TSR=4 and -6^0 blade pitch angle.

The amount of torque is more stable in TSR = 5 because the attack angle acts near the optimum lift to drag ratio. At TSR 5, the maximum value of torque occurred in the 0^0 blade pitch angle. In the blade pitch angle less than 0^0, the attack angle is large, reduction in the lift to drag ratio occurred and torque decreases. In the blade pitch angle more than 0^0, the attack angle is decreased, and it leads to an increase in TKE, the flow doesn't move along the surface and torque reduces.

Fig 11. depicts torque versus TSR in different blade pitch angles. The maximum value of torque happened between -2^0 and 2^0 blade pitch angles. In those angles, the blade has more resistance under the variation of TSR. In 6^0 and 4^0 blade pitch angles, the attack angles are low, so by decreasing the TSR, attack angle increases and conducts better lift to drag ratio and torque improves. The trend is inverse for -4^0 and -6^0 blade pitch angle concerning the 6^0 and 4^0. In these conditions, the value of the attack angle is high, so increasing the TSR decreases the attack angle and improves the torque.

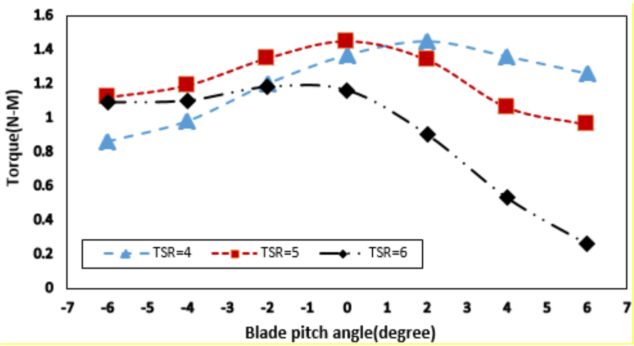

Fig 10: Torque versus to blade pitch angle in different TSRs

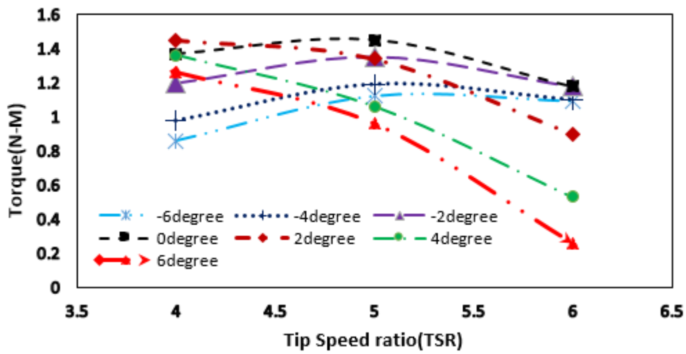

Fig 11: Torque versus to TSR in different blade pitch angles

Fig 12. shows the C_p versus the blade pitch angle in different TSRs. As expected, in most of the blade pitch angles, the maximum amount of C_p has occurred in the maximum torque achievement. However, in some situations increasing and decreasing in TSRs, leads to enhancement and reduction in C_p. For example, in $+6^0$ blade pitch angle, although the amount of torque was more than TSR 5 is less than TSR 4, but the increase in angular velocity leads to improvement of Cp at TSR 5 and reduced the discrepancy of C_p between them (6^0 blade pitch angle, TSR 4 and TSR 5). This condition happened at TSR 5 and TSR 6 in the 0^0 blade pitch angle.

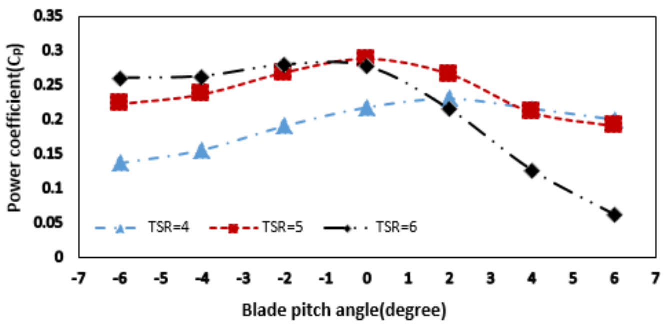

Fig 12: Curves of Cp to blade pitch angle in different TSRs

Fig 13. depicts the C_p versus TSR in different blade pitch angles. In a 2^0 blade pitch angle, the maximum value of torque occurs in TSR 4, but increasing in angular velocity in TSR 5, leads to having a better performance with respect to TSR 4. In 0^0 blade pitch angle, although the amount of torque in TSR 4 is more than TSR 6, the increase in angular velocity leads to achieving better performance in TSR 6. The maximum amount of velocity is observed in TSR 5 and 0^0 blade pitch angle. Besides, the C_p has more stability due to place in equilibrium conditions of blade pitch angle and TSR which they performed an optimum attack angle.

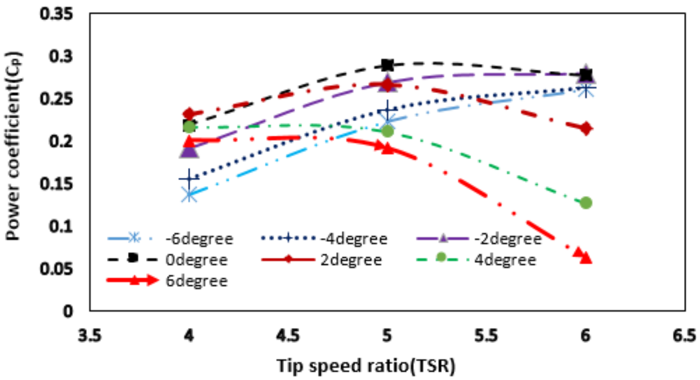

Fig 13: Curves of Cp to TSR in different blade pitch angle

6 Conclusions

In this investigation, a 2-Bladed HATCT was simulated in -6^0 till +6^0 in $4 \leq TSR \leq 6$. A computational analysis is carried out to assess the performance of turbines using CFD through ANSYS-FLUENT software. For turbulence modeling, the SST-k-ω model was used. The fluid was considered as incompressible flow and a steady-state condition. The results indicated that the maximum amount of C_P (0.26) occurs at TSR 5 and 0^0 blade pitch angle. For the design a 2-Bladed pitch-able HATCT based on the simulations, there are remarkable relationships which shows that the decreasing in C_p due to increase in TSR, can be compensated by decreasing in blade pitch angle. Also, decreasing in C_p due to decrease in TSR, can be controlled by increasing of blade pitch angle.

7 Acknowledgment

The research was supported by the Ministry of Education, Youth, and Sports of the Czech Republic and the European Union (European Structural and Investment Funds Operational Program Research, Development, and Education) in the framework of the project "Modular platform for autonomous chassis of specialized electric vehicles for freight and equipment transportation", Reg. No. CZ.02.1.01/0.0/0.0/16_025/0007293.

8 References

1. Abuan, B.E. and R.J. Howell, *The performance and hydrodynamics in unsteady flow of a horizontal axis tidal turbine.* Renewable Energy, 2019. 133: p. 1338-1351. https://doi.org/10.1016/j.renene.2018.09.045

2. Frost, C., et al., *The effect of tidal flow directionality on tidal turbine performance characteristics.* Renewable Energy, 2015. 78: p. 609-620. https://doi.org/10.1016/j.renene.2015.01.053
3. Funke, S.W., P.E. Farrell, and M. Piggott, *Tidal turbine array optimisation using the adjoint approach.* Renewable Energy, 2014. 63: p. 658-673. https://doi.org/10.1016/j.renene.2013.09.031
4. Tian, W., Z. Mao, and H. Ding, *Design, test and numerical simulation of a low-speed horizontal axis hydrokinetic turbine.* International Journal of Naval Architecture and Ocean Engineering, 2018. 10(6): p. 782-793. https://doi.org/10.1016/j.ijnaoe.2017.10.006
5. Alipour, R., et al., *Performance improvement of a new proposed Savonius hydrokinetic turbine: a numerical investigation.* Energy Reports, 2020. 6: p. 3051-3066. https://doi.org/10.1016/j.egyr.2020.10.072
6. Uihlein, A. and D. Magagna, *Wave and tidal current energy–A review of the current state of research beyond technology.* Renewable and Sustainable Energy Reviews, 2016. 58: p. 1070-1081. https://doi.org/10.1016/j.rser.2015.12.284
7. *https://marineenergy.biz.*
8. *https://www.power-technology.com/.*
9. Morandi, B., et al., *Experimental investigation of the near wake of a horizontal axis tidal current turbine.* International Journal of Marine Energy, 2016. 14: p. 229-247. https://doi.org/10.1016/j.ijome.2016.02.004
10. Fituri, A., H.H. Aly, and M. El-Hawary, *Unsteady surface wave influence on tidal current power forecasting.* Ocean Engineering, 2020. 218: p. 108231. https://www.x-mol.com/paperRedirect/1318715687781502976
11. Deng, G., et al., *Prospective of development of large-scale tidal current turbine array: An example numerical investigation of Zhejiang, China.* Applied Energy, 2020. 264: p. 114621. https://doi.org/10.1016/j.apenergy.2020.114621
12. Jo, C.-H., et al., *Performance analysis of a HAT tidal current turbine and wake flow characteristics.* Renewable energy, 2014. 65: p. 175-182. https://doi.org/10.1016/j.renene.2013.08.027
13. Tarver, B.T., J.C. Chan, and C.H. Jo, *A new concept in tidal turbines.* International Journal of Energy Research, 2016. 40(5): p. 579-586. https://doi.org/10.1002/er.3440
14. hee Jo, C., et al., *Performance of horizontal axis tidal current turbine by blade configuration.* Renewable Energy, 2012. 42: p. 195-206. https://doi.org/10.1016/j.renene.2011.08.017
15. Münch-Alligné, C., et al., *Experimental assessment of a new kinetic turbine performance for artificial channels.* Water, 2018. 10(3): p. 311. https://doi.org/10.3390/w10030311
16. Yan, J., et al., *Free-surface flow modeling and simulation of horizontal-axis tidal-stream turbines.* Computers & Fluids, 2017. 158: p. 157-166. https://doi.org/10.1016/j.compfluid.2016.06.016
17. Alipour, R., et al., *On the Performance of Small-Scale Horizontal Axis Tidal Current Turbines. Part 1: One Single Turbine.* Sustainability, 2020. 12(15): p. 5985. https://doi.org/10.3390/su12155985
18. Goundar, J.N. and M.R. Ahmed, *Design of a horizontal axis tidal current turbine.* Applied energy, 2013. 111: p. 161-174. https://doi.org/10.1016/j.apenergy.2013.04.064

19. Huang, B., G. Zhu, and T. Kanemoto, *Design and performance enhancement of a bi-directional counter-rotating type horizontal axis tidal turbine.* Ocean Engineering, 2016. 128: p. 116-123. https://doi.org/10.1016/j.oceaneng.2016.10.012
20. Zhu, F.-w., et al., *Blade design and optimization of a horizontal axis tidal turbine.* Ocean Engineering, 2020. 195: p. 106652. https://doi.org/10.1016/j.oceaneng.2019.106652
21. Wani, F., et al., *Lifetime Analysis of IGBT Power Modules in Passively Cooled Tidal Turbine Converters.* Energies, 2020. 13(8): p. 1875. https://doi.org/10.3390/en13081875
22. de Jesus Henriques, T.A., et al., *The influence of blade pitch angle on the performance of a model horizontal axis tidal stream turbine operating under wave–current interaction.* Energy, 2016. 102: p. 166-175. https://doi.org/10.1016/j.energy.2016.02.066
23. Rocha, P.C., et al., *k–ω SST (shear stress transport) turbulence model calibration: A case study on a small scale horizontal axis wind turbine.* Energy, 2014. 65: p. 412-418. https://doi.org/10.1016/j.energy.2013.11.050
24. Tatum, S., et al., *Wave–current interaction effects on tidal stream turbine performance and loading characteristics.* International Journal of Marine Energy, 2016. 14: p. 161-179. https://doi.org/10.1016/j.ijome.2015.09.002
25. Jing, F.-m., et al., *Experimental study of hydrodynamic performance of full-scale horizontal axis tidal current turbine.* Journal of Hydrodynamics, Ser. B, 2017. 29(1): p. 109-117. https://doi.org/10.1016/S1001-6058(16)60722-9
26. Alipour, R., Alipour, R., Fardian, F., & Hossein Tahan, M. (2022). Optimum performance of a horizontal axis tidal current turbine: A numerical parametric study and experimental validation. Energy Conversion and Management, 258 doi:10.1016/j.enconman.2022.115533